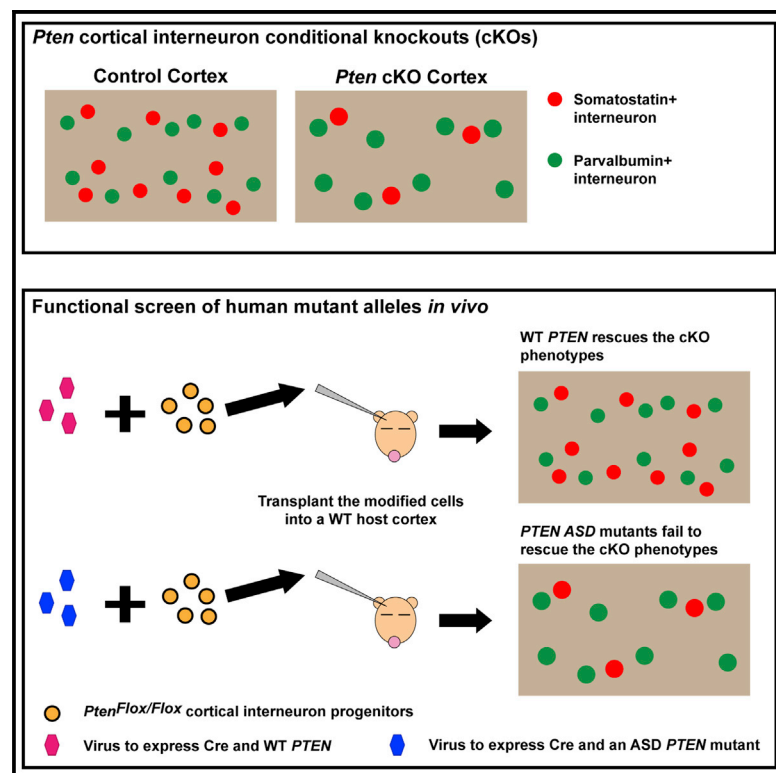


The Parvalbumin/Somatostatin Ratio Is Increased in *Pten* Mutant Mice and by Human *PTEN* ASD Alleles

Graphical Abstract



Authors

Daniel Vogt, Kathleen K.A. Cho, ..., Vikaas S. Sohal, John L.R. Rubenstein

Correspondence

daniel.vogt@ucsf.edu (D.V.), john.rubenstein@ucsf.edu (J.L.R.R.)

In Brief

Vogt et al. develop an *in vivo* method to efficiently screen human alleles of ASD genes, using *PTEN* as a proof of principle. They also show that mouse *Pten* differentially regulates cortical interneuron development and is necessary for the survival of those that express somatostatin.

Highlights

- *Pten* regulates the ratio of PV⁺/SST⁺ cortical interneurons
- Loss of *Pten* increases PV⁺ process growth and inhibition
- *Pten* interneuron cKOs have altered social behavior and gamma oscillations
- An *in vivo* screening assay tests human ASD allele function



The Parvalbumin/Somatostatin Ratio Is Increased in *Pten* Mutant Mice and by Human *PTEN* ASD Alleles

Daniel Vogt,^{1,3,*} Kathleen K.A. Cho,^{1,4,5} Anthony T. Lee,^{1,4,5} Vikaas S. Sohal,^{1,4,5} and John L.R. Rubenstein^{1,2,3,*}

¹Department of Psychiatry

²Neuroscience Program

³Nina Ireland Laboratory of Developmental Neurobiology

University of California, San Francisco, San Francisco, CA 94158, USA

⁴Center for Integrative Neuroscience

⁵Sloan-Swartz Center for Theoretical Neurobiology

University of California, San Francisco, San Francisco, CA 94143, USA

*Correspondence: daniel.vogt@ucsf.edu (D.V.), john.rubenstein@ucsf.edu (J.L.R.R.)

<http://dx.doi.org/10.1016/j.celrep.2015.04.019>

This is an open access article under the CC BY-NC-ND license (<http://creativecommons.org/licenses/by-nc-nd/4.0/>).

SUMMARY

Mutations in the phosphatase *PTEN* are strongly implicated in autism spectrum disorder (ASD). Here, we investigate the function of *Pten* in cortical GABAergic neurons using conditional mutagenesis in mice. Loss of *Pten* results in a preferential loss of SST⁺ interneurons, which increases the ratio of parvalbumin/somatostatin (PV/SST) interneurons, ectopic PV⁺ projections in layer I, and inhibition onto glutamatergic cortical neurons. *Pten* mutant mice exhibit deficits in social behavior and changes in electroencephalogram (EEG) power. Using medial ganglionic eminence (MGE) transplantation, we test for cell-autonomous functional differences between human *PTEN* wild-type (WT) and ASD alleles. The *PTEN* ASD alleles are hypomorphic in regulating cell size and the PV/SST ratio in comparison to WT *PTEN*. This MGE transplantation/complementation assay is efficient and is generally applicable for functional testing of ASD alleles in vivo.

INTRODUCTION

Autism spectrum disorder (ASD) is characterized by deficits in language, social interactions, and repetitive behaviors. Some forms of ASD may be caused by an imbalance in excitatory/inhibitory (E/I) tone in the brain (Rubenstein and Merzenich, 2003). An increasing number of ASD genetic risk loci are being identified (Murdoch and State, 2013; Tebbenkamp et al., 2014). Recent data from mouse models, including *MeCP2* (Chao et al., 2010), *Scn1a* (Han et al., 2012), *Caspr2* (Peñagarikano et al., 2011), *Caspr4* (Karayannis et al., 2014), and *Shank3* and the mouse strain BTBR (Gogolla et al., 2014), showed defects in GABAergic neurons that contribute to ASD phenotypes by altering E/I balance. This balance may be disrupted by altering the relative numbers, functions, and/or connectivity between excitatory neurons and inhibitory interneurons.

In the neocortex, glutamatergic excitatory neurons comprise ~70% of all neurons, and GABAergic inhibitory interneurons account for ~30%. The majority of interneurons arise from the medial and caudal ganglionic eminences (MGE and CGE) of the basal ganglia. Immature interneurons tangentially migrate from the MGE to the cortex, then radially migrate into cortical layers (Anderson et al., 1997). As MGE cells mature, they express specific molecular markers of interneuron subtypes, including somatostatin (SST) and parvalbumin (PV) (Wonders and Anderson, 2006). CGE-derived interneurons express vasoactive intestinal peptide (VIP) and Reelin (which lack SST) (Miyoshi et al., 2010). Furthermore, interneuron subgroups project to different cortical layers and synapse within distinct domains of the neocortex (Huang et al., 2007). Thus, perturbations in different interneuron subgroups can lead to E/I imbalance by a variety of mechanisms.

While most ASD genes individually account for <1% of the genetic risk, some genes, including the phosphatase *PTEN*, are more often mutated in ASD (O’Roak et al., 2012). *PTEN* inhibits phosphatidylinositol 3-kinase (PI3K)/Akt signaling after its activation by receptor tyrosine kinases (RTKs) and other receptors (Bourgeron, 2009; Stiles, 2009). The growth-promoting Akt/mTor signaling cascade is also a hub for other ASD candidate genes, including *Tsc1* and *Tsc2* (Wiznitzer 2004) and *NF1* (Marui et al., 2004; Mbarek et al., 1999).

Pten is broadly expressed in the developing and adult mouse brain, including in glutamatergic and GABAergic neurons (herein and Ljungberg et al., 2009). *Pten* regulates many developmental processes, including migration (Kölsch et al., 2008), growth and morphogenesis (Kwon et al., 2006), and synaptic dynamics (Fraser et al., 2008; Luikart et al., 2011; Williams et al., 2015). Conditional deletion of *Pten* in excitatory cortical neurons results in macrocephaly and overgrowth of cortical cell bodies (somas), axons, and dendrites and leads to social interaction deficits; some of these features were rescued by pharmacologic inhibition of the mTor pathway (Kwon et al., 2006; Zhou et al., 2009). However, the role of *Pten* and other genes in the Akt/mTor pathway is poorly understood in GABAergic cortical interneuron development.

Here, we investigated *Pten* function during cortical interneuron development. Loss of *Pten* led to altered distribution of

MGE-derived cells, neonatal interneuron death, and an overall loss in interneurons. However, preferential loss of SST⁺ interneurons led to an increased ratio of PV/SST in surviving interneurons in the adult mutant cortex, with ectopic PV⁺ processes in layer I. Many of these phenotypes were cell autonomous. We also developed a method to virally modify MGE cells before transplantation to study the function of human ASD alleles and found that *P TEN* ASD alleles were hypomorphic for multiple phenotypes.

RESULTS

Pten Loss in the MGE Leads to Increased AKT Signaling

To determine its role in GABAergic cortical interneuron development, we generated *Pten* conditional knockouts (cKOs) from the MGE and preoptic area (POA) progenitors by crossing *Pten*^{Flox} (Suzuki et al., 2001) to *Nkx2.1-Cre* (Xu et al., 2008) mice. The *Ai14* Cre-dependent reporter (Madisen et al., 2010) was used to follow cells that expressed Cre (tdTomato is expressed after Cre-mediated recombination). The *Nkx2.1-Cre* BAC transgenic drives expression, beginning on approximately embryonic day 9.5 (E9.5), in most of the ventricular zone (VZ) of the MGE and POA (Figures S1A–S1C). At E12.5, *Pten* was globally expressed in the brains of WT and *Pten*^{Flox/+} mice, including in the MGE (Figures S1D, S1E, S1G, and S1H). Efficient loss of *Pten* protein occurred in early progenitors of the VZ and their progeny in the *Nkx2.1-Cre*-lineage domains (Figures S1C, S1F, and S1I).

Since loss of *Pten* leads to increased phosphorylated Akt (pAkt) and pGSK3beta in neurons (Kwon et al., 2006), we probed E13.5 MGE tissues for pAKT and pGSK3beta. Indeed, pAkt was increased ~3.5-fold at serine⁴⁷³ ($p = 0.02$) and ~3-fold at threonine³⁰⁸ ($p = 0.01$) (Figure S1J). Moreover, pGSK3beta at serine⁹ was increased ~1.6-fold in *Pten* cKOs ($p = 0.03$) (Figure S1J). These data demonstrate a role for *Pten* signaling in regulating the Akt pathway in the embryonic MGE.

Pten Loss in GABAergic Cortical Interneuron Progenitors Differentially Effects SST and PV Interneurons

Nkx2.1-Cre⁺; *Pten* cKOs survive into adulthood but weighed ~25% less than their WT and *Pten*^{Flox/+} littermates at postnatal day 30 (P30) (Figure 1A). In contrast to other *Pten* mutants (Kwon et al., 2006), the brains of *Nkx2.1-Cre*⁺; *Pten* cKOs were not altered in shape or size (Figure 1A). First, we counted the number of *Nkx2.1-Cre*-lineage cortical interneurons in the somatosensory cortex. At P30, there was an ~53% reduction in the total number of *Nkx2.1-Cre*-lineage cells (Figures 1B–1G and 1H; Table S1). Next, we assessed the proportion of the two main subgroups of MGE-derived interneurons via expression of SST and PV in the remaining tdTomato⁺ cells. The percentage of tdTomato⁺ cells that were SST⁺ decreased 34% in *Pten* cKO neocortices (Figures 1B–1G and 1I; $p = 0.01$). Yet, the percentage of tdTomato⁺ cells that were PV⁺ increased 39% (Figures 1E–1G and 1J; $p = 0.009$). This disproportionate effect on SST⁺ and PV⁺ interneuron numbers resulted in a greater PV to SST ratio in the P30 cortex (Figure 1K; $p = 0.01$), as well as in striatum and hippocampus (Table S1). Moreover, in *Pten* cKOs, the SST⁺ neuropil was greatly reduced in layer I, whereas

the PV⁺ neuropil, which normally was restricted to neocortical layers II–VI, ectopically projected into layer I and displayed prominent PV⁺ puncta (Figures 1E'–1G').

Nkx2.1-Cre removed *Pten* from the stem cells in the VZ. Next, we used *Dlx12b-Cre* (Potter et al., 2009) to remove *Pten* from secondary progenitors in the subventricular zone (SVZ) of the entire subpallium. At E15.5, *Pten* protein was detected in the VZ, but not the SVZ or neuronal layers of the basal ganglia (Figures S2A–S2A'' and S2B–S2B''). At P18, the percentage of tdTomato⁺ cells that expressed VIP, a marker of CGE-derived interneurons, was unchanged (Figures S2C–S2E and S2L).

Similar to *Nkx2.1-Cre* cKOs, the percentage of tdTomato⁺ cells in the *Dlx12b-Cre* cKOs that expressed SST decreased by 32% (Figures S2F–S2H and S2M; $p = 0.004$). Moreover, there was a trend for an increased percentage of tdTomato⁺ cells that expressed PV (increased 24%, but did not reach statistical significance) (Figures S2I–S2K and S2N). Like the *Nkx2.1-Cre* cKOs, there was a trend for fewer total tdTomato⁺ cells in the neocortex (Figure S2O). Overall, *Dlx12b-Cre* cKOs had an increased PV⁺/SST⁺ ratio of neocortical interneurons (Figure S2P; $p = 0.01$). These mutants also had ectopic PV⁺ projections in neocortical layer I at P18 (Figures S2I'–S2K'). Unfortunately, these mice could not be analyzed at later stages, because they die soon after P18 for unknown reasons.

Pten Loss In Progenitors, but Not Postmitotic Interneurons, Decreased SST⁺ Numbers

Pten loss, beginning in either the VZ (*Nkx2.1-Cre*) and/or SVZ (*Dlx12b-Cre*), led to a preferential loss of SST⁺ interneurons, while PV⁺ interneurons composed most of the remainder. To test if *Pten* was required in postmitotic SST⁺ cells, we used a *SST-IRES-Cre* mouse line (Taniguchi et al., 2011), which expresses Cre in MGE-derived SST⁺ cells as they leave the MGE (Figure 2A). Somatosensory cortices were assessed at P30 for *SST-IRES-Cre*-lineages (tdTomato⁺). In contrast to *Nkx2.1-Cre* and *Dlx12b-Cre* *Pten* cKOs, *SST-IRES-Cre* cKOs did not show interneuron loss (Figure 2H), had no change in the percentage of tdTomato⁺ interneurons that were SST⁺ or PV⁺ (Figures 2B–2I), and had no ectopic PV⁺ neuropil in layer I (Figures 2E–2G). These data demonstrate that the *Pten* phenotypes observed using *Nkx2.1-Cre* and *Dlx12b-Cre* are caused by *Pten* loss in progenitor cells, which in turn led to changes in the PV/SST ratio.

Normal Proliferation in *Pten* cKOs

The reduced numbers of interneurons in the neocortex of *Nkx2.1-Cre*⁺; *Pten*^{Flox/Flox} cKOs could be due to altered proliferation or apoptosis. We evaluated proliferation in the MGE by assessing phospho-histone-3 (PH3) expression and 5-ethynyl-2'-deoxyuridine (EdU) incorporation, measures of M and S phase, respectively. The total number of PH3⁺ cells within the VZ and SVZ of the *Nkx2.1-Cre* domain of the MGE (tdTomato⁺) was counted at E11.5, E12.5, and E15.5; no changes in PH3⁺ cells were found (Figures S3A–S3I). Next, we administered a 30-min pulse of EdU at E11.5, E12.5, and E15.5 and counted the density of EdU⁺ cells in the MGE's VZ and SVZ MGE. Lack of *Pten* had no effect (Figures S3J–S3R), suggesting normal proliferation.

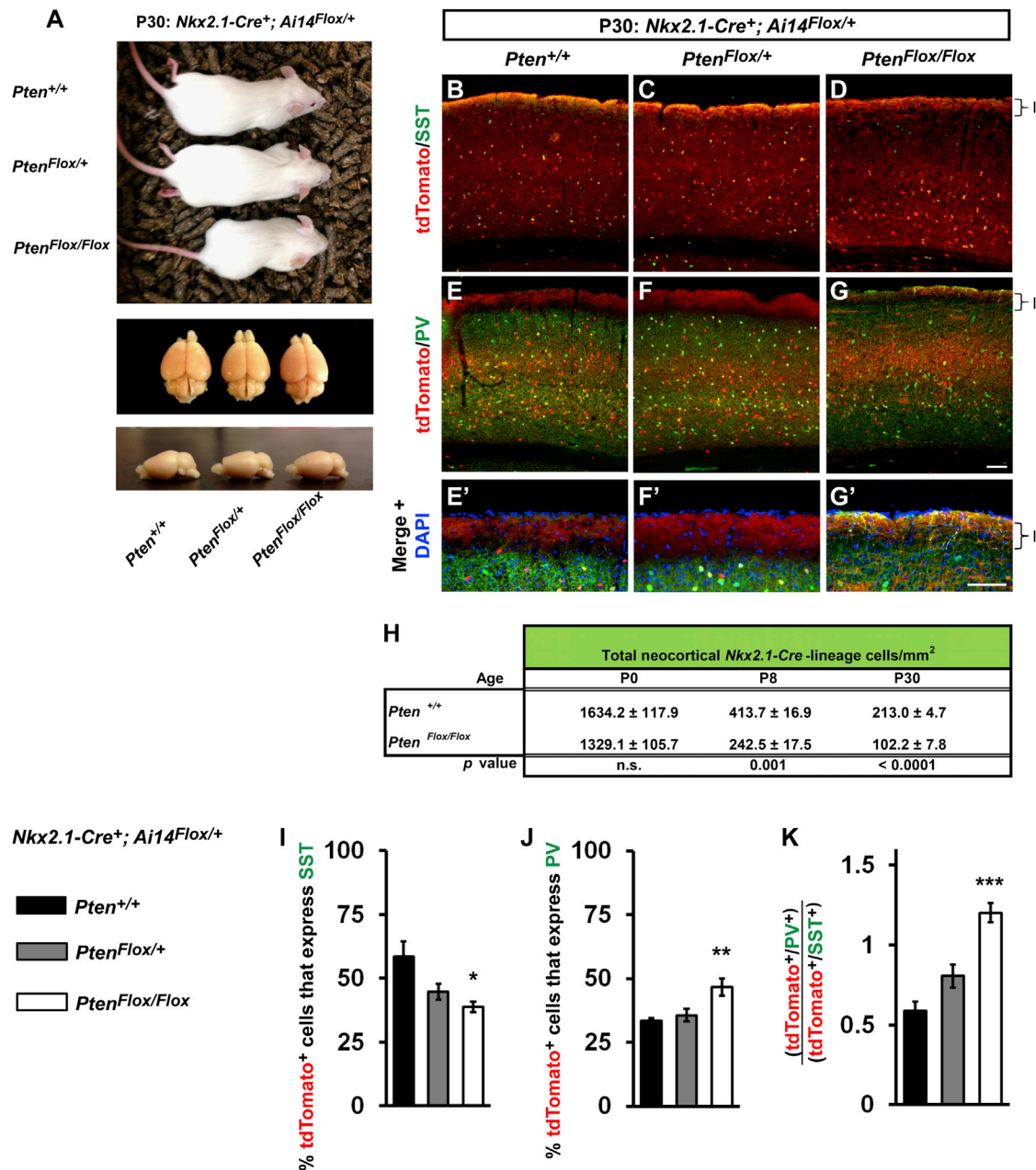


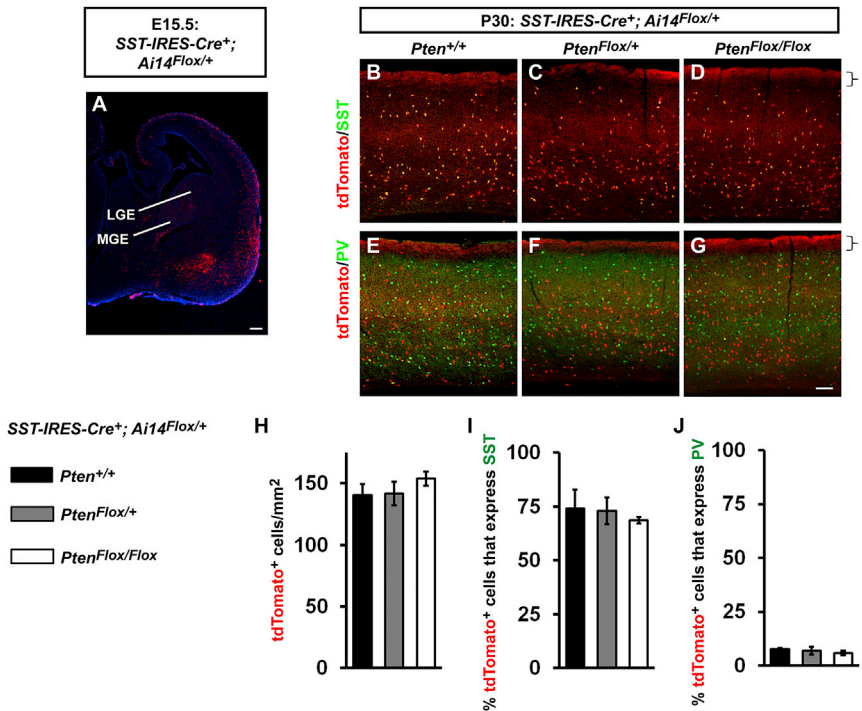
Figure 1. *Nkx2.1-Cre; Pten* Conditional Mutants Exhibit Reduced Interneuron Numbers, Increased PV/SST Ratio, and Ectopic PV Processes in Layer I

(A) Images of postnatal day 30 (P30) mice and brains (superior and lateral views) from *Pten^{+/+}*, *Pten^{Flox/+}*, and *Pten^{Flox/Flox}* (*Nkx2.1-Cre⁺; Ai14^{Flox/+}*) genotypes. (B–G) Coronal immunofluorescent images of P30 somatosensory cortices show coexpression of tdTomato with SST (B–D) or with PV (E–G). (E'–G') Higher-magnification images of neocortical layer I from images (E)–(G) that have been merged with DAPI. Brackets to the right of each panel denote the boundaries of layer I. (H) Quantification of the number of tdTomato⁺ cells per square millimeter (mm²) in the somatosensory cortex over time. (I and J) Quantification of the percentage of tdTomato⁺ cells that express either SST (I) or PV (J). (K) Ratio of tdTomato⁺/PV⁺ cells per mm² over tdTomato⁺/SST⁺ cells per mm² in the neocortex. Data are presented as mean ± SEM. **p* < 0.05, ***p* < 0.01. Scale bars in (G) and (G') represent 100 μm. See also Figures S1 and S2 and Tables S1 and S2.

Differential Distribution and Death of SST⁺ Cells in *Pten* cKOs

To determine if *Pten* cKOs showed early changes in cell fate, we assessed the proportion of tdTomato⁺ cells that expressed SST

at E12.5 and E15.5. At E12.5, there were no changes in the number or proportion of SST⁺ cells assayed using in situ hybridization or antibody staining (data not shown). However, by E15.5, the percentage of tdTomato⁺ cells that expressed SST was



increased ~45% in the lateral cortex (Figures 3A–3I; $p = 0.02$) and decreased ~30% in the neocortex (Figures 3A, 3B, and 3J–3P; $p = 0.006$ total, $p = 0.002$ MZ, $p = 0.02$ CP), suggesting that SST⁺ cKO interneurons were biased to occupy the lateral cortex.

Next, we assessed if *Pten* cKO cortical interneurons were susceptible to apoptosis by testing for expression of cleaved caspase-3 (cC3). While we did not detect changes in apoptosis at E15.5, by E17.5, cC3⁺ cells were readily detected in ~13% of tdTomato⁺ marginal zone (MZ) *Pten* cKO cells in both the neocortex and lateral cortex (controls had <1%; data not shown). By P0, ~36% of *Pten* cKO tdTomato⁺ cells in the MZ of the lateral cortex were cC3⁺ (Figures 3Q–3V and 3X; $p < 0.001$).

In the postnatal neocortex, there was progressive loss of MGE-derived (tdTomato⁺) interneurons in the *Pten* cKOs: 10% at P0, 47% at P8, and 53% at P30 (Figure 1H). Thus, interneuron apoptosis primarily occurred between E17.5 and P8. Interestingly, apoptosis was restricted to the cortical MZ, suggesting that interneuron death may occur due to an inability to integrate into the cortex.

Finally, we asked if SST⁺ or SST[−] interneurons were differentially affected by apoptosis, by calculating the percentage of cC3⁺/tdTomato⁺ cells in the MZ that were either SST⁺ or SST[−]. Although SST[−] cells were cC3⁺, cC3⁺/tdTomato⁺ cells in the MZ of *Pten* cKOs were ~2-fold more likely to be SST⁺ (Figure 3X; $p < 0.001$ all conditions). This provided evidence that SST⁺ interneurons lacking *Pten* are more susceptible to apoptosis than SST[−] interneurons. Moreover, at P0, the percentage of tdTomato⁺ cells that expressed SST in the lateral cortex was reduced 26% (Figure 3W; $p = 0.02$), consistent with the evidence noted above that this was the period of interneuron death.

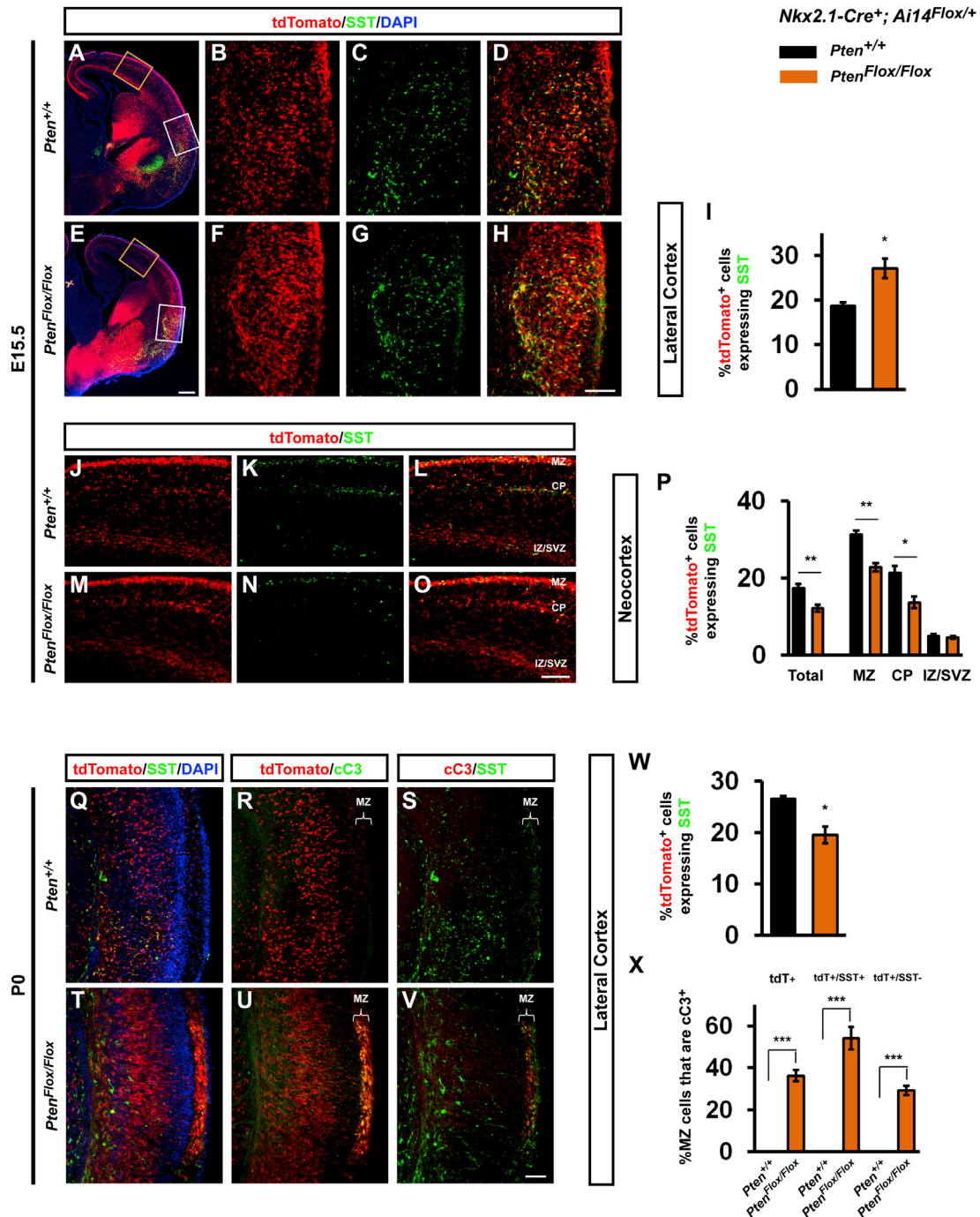
Since SST⁺ and PV⁺ neurons are the two primary MGE-derived cell types, the tdTomato⁺/SST[−] cells are likely to

become PV⁺ cells. Although there is no early marker for PV⁺ interneurons, there is evidence that the majority of immature MGE cells that express SST will become SST⁺. (Taniguchi et al., 2011; Vogt et al., 2015). Thus, prenatal expression of SST in the MGE-lineage is correlated with a SST⁺ fate, and we propose that SST⁺ embryonic *Pten* cKO cells are more susceptible to apoptosis than those that are SST[−] (likely PV⁺ fate).

Nkx2.1-Cre; Pten cKOs Exhibit Increased Inhibition onto Neocortical Pyramidal Neurons, Deficits in Social Interaction, and Changes in Electroencephalogram Gamma Oscillations

We next examined if *Pten* loss in interneurons altered the amount of inhibition received by neocortical excitatory neurons. Electrophysiological recordings were made of inhibitory inputs onto excitatory neurons in neocortical layers II/III at P30 (schema, Figure 4A). Despite the loss of half of the MGE-derived interneurons (Figure 1), there was an ~2-fold increase in the frequency of spontaneous inhibitory postsynaptic currents (IPSCs) onto layer II/III excitatory neurons in *Nkx2.1-Cre; Pten^{Flox/Flox}* mice (Figure 4C; $p = 0.02$) but no change in amplitude between groups (Figure 4D). Example IPSC recordings are shown for *Pten^{+/+}* and *Pten^{Flox/Flox}* (Figure 4B). These data demonstrate that spontaneous inhibitory tone is increased in layers II/III of *Pten* mutants.

Next, we performed a series of behavioral assays on *Nkx2.1-Cre; Pten* cKOs at P30. *Pten* cKOs were similar to WTs in the open field (Figures 5A–5C) and the elevated plus maze (Figures 5D and 5E), suggesting normal levels of exploratory activity, locomotion, and anxiety. However, *Pten* cKOs spent less time with novel mice in a social interaction test (Figure 5F; $p = 0.03$) and with a novel object (Figure 5I; $p = 0.05$). Interestingly, *Pten* cKOs had elevated electroencephalogram (EEG) power during social interaction, with the greatest effect in the gamma frequency range (Figure 5G; $p = 0.005$). The baseline EEG was also recorded before the social interaction test and exhibited



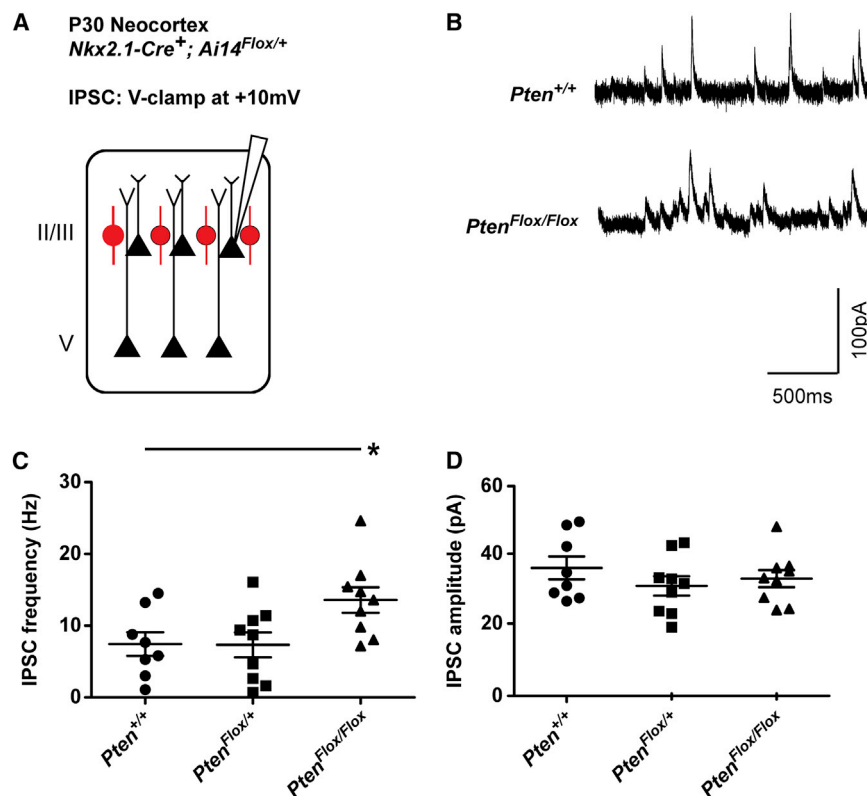


Figure 4. Neocortical Principle Neurons in *Nkx2.1-Cre; Pten* cKOs Received Increased IPSC Frequency

(A) Schema of neocortical recordings performed on principle neurons in somatosensory cortical layers II/III (black) from *Nkx2.1-Cre⁺; Ai14^{Flox/+}; Pten^{+/+}, Pten^{Flox/+}, or Pten^{Flox/Flox}* slices at P30. *Nkx2.1-Cre⁺* interneurons were tdTomato⁺ (red). (B) Example traces of inhibitory postsynaptic currents (IPSCs) from *Pten^{+/+}* and *Pten^{Flox/Flox}* slices. (C and D) Quantification of IPSC frequency onto principle neurons (C) and IPSC amplitude (D). Data are presented as mean \pm SEM. * $p < 0.05$.

less power in the gamma frequency range in *Pten* cKOs (Figure 5H; $p = 0.04$). Overall, these data demonstrated that loss of *Pten* in cortical interneurons results in abnormal social behavior and altered EEG oscillations, within the gamma frequency band, both at baseline and during a task.

Cell-Autonomous Role for *Pten* in Regulating Cortical Interneuron Soma Size and Interneuron Subgroup Ratios

To assess the cell-autonomous role for *Pten* on cortical interneuron development, we utilized an MGE cell transplantation assay (Alvarez-Dolado et al., 2006). E12.5 *Dlx12b-Cre⁺; Ai14^{Flox/+}* MGE cells from *Pten^{+/+}, Pten^{Flox/+}, or Pten^{Flox/Flox}* embryos were transplanted into wild-type (WT) P1 host neocortices and assessed at 35 days posttransplant (DPT) (Figure 6A). Transplanted *Pten^{Flox/Flox}* MGE cells had increased soma area (Figures 6B–6G) compared to both *Pten^{+/+}* and *Pten^{Flox/+}* (Figure 6H; $p < 0.0001$, both conditions).

Similar to the cKOs, transplanted *Pten* cKO MGE cells had a decreased proportion of SST⁺ cells (Figures 6B–6D and 6I; *Pten^{Flox/+}* $p = 0.002$, *Pten^{Flox/Flox}* $p = 0.0001$) and increased PV⁺ cells (Figures 6E–6G and 6J; $p = 0.02$). The transplanted MGE cells were also assayed for proteins that are expressed in specific MGE-derived interneuron groups: KV3.1, a channel predominantly expressed in PV⁺ fast-spiking neurons (Du et al., 1996), as well as Reelin and Npas1 (which are expressed in a subpopulation of SST⁺, but not PV⁺, interneurons) (Pesold et al., 1999; Stanco et al., 2014). The percentage of transplanted *Pten^{Flox/Flox}* MGE cells that expressed KV3.1 was increased (Figures S4A,

S4D, and S4G; $p = 0.001$). In conjunction, the percentage of cells expressing Reelin (Figures S4B, S4E, and S4H; $p = 0.01$) and Npas1 (Figures S4C, S4F, and S4I; $p = 0.006$) was decreased in *Pten^{Flox/Flox}* MGE transplants, consistent with a reduction of SST⁺ interneurons.

We next assessed the cell-intrinsic physiological properties of the transplanted cells at 45 DPT (Table S3). Despite decreased AP threshold and resting membrane potential in transplanted *Pten* cKO MGE cells, the majority of cell-intrinsic firing properties (i.e., frequency-input current slope, adaption ratio, and action potential half-width) between WT and *Pten* cKOs were similar. Together with the ectopic PV⁺ processes in neocortical layer I and increased IPSC frequency onto excitatory neurons, these data suggest that *Pten* cKO cells primarily increased inhibitory tone via an overgrowth mechanism rather than by increased cell-intrinsic excitability.

An In Vivo Complementation Assay of *PTEN* ASD Alleles Demonstrates Functional Deficits in Cortical Interneuron Development

Since the increased PV/SST ratio was a prominent phenotype in multiple brain regions (Table S1) and was cell autonomous (Figure 6), it was an ideal phenotype to test if human *PTEN* ASD alleles were functionally deficient. A major roadblock in ASD research is the lack of efficient screening assays for human alleles found in autism populations, particularly those with the power to test allele function in vivo during brain development. To circumvent this problem, we improved upon methods to introduce genes of interest into MGE cells before transplantation for in vivo development (Vogt et al., 2014) that combine Cre-dependent gene deletion and activation of a fluorescent reporter in the transduced MGE cells (Vogt et al., 2015) with expression of an allele. In this manner, a WT or ASD allele is expressed while simultaneously deleting the corresponding endogenous gene. First, donor MGE cells that harbor a floxed gene of interest are transduced with a lentivirus, then transplanted into a WT host, allowing the modified cells to develop in vivo. This strategy challenges an ASD allele to complement

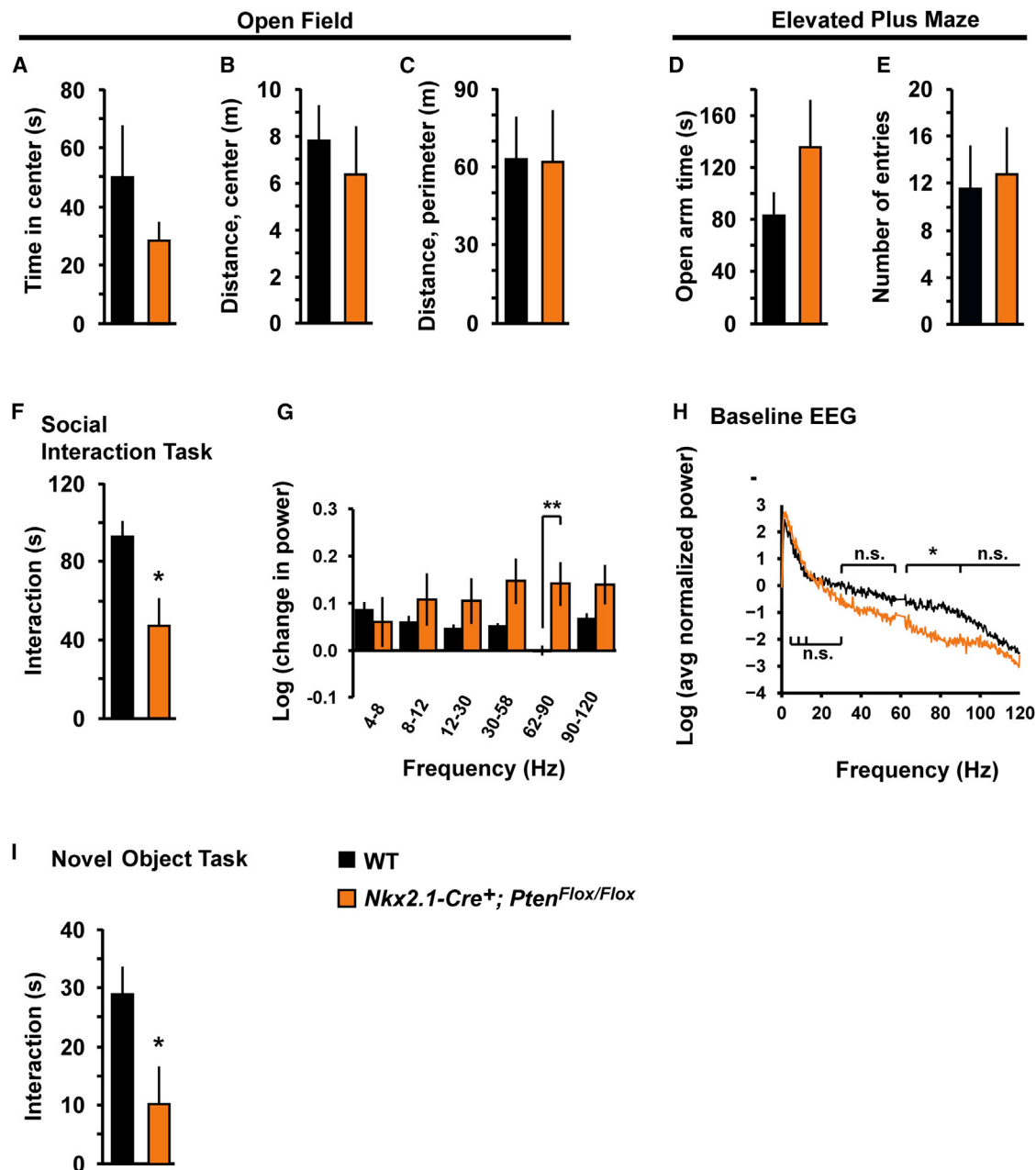


Figure 5. *Nkx2.1-Cre; Pten* cKOs Showed Reduced Social Behavior and Altered EEG Gamma Oscillations

(A–C) Open-field test: quantification of P30 *Nkx2.1-Cre⁺; Pten^{+/+}* (WT) and *Pten^{flox/flox}* littermates for time spent in the center of the field (A) and distance traveled in the center (B) and perimeter (C).

(D and E) Elevated plus maze: quantification of the time spent in open arms (D) and the number of entries made (E).

(F) Social interaction task: quantification of the amount of social interaction time *Nkx2.1-Cre⁺; Pten^{+/+}* (WT) and *Pten^{flox/flox}* littermates spent with a stranger mouse.

(G) Social interaction task: quantification of changes in electroencephalogram (EEG) power, log transformed, during periods of social interaction. Graph represents recordings made from prefrontal cortex; significant changes were in the high- γ range (62–90 Hz).

(H) Prefrontal EEG, shown as the log transform of the averaged, normalized power spectrum. The graph was analyzed from a period before the social interaction test and the power spectrum from each mouse was normalized by the sum of all values from 0 to 120 Hz (excluding 58–62 Hz). *Nkx2.1-Cre; Pten^{flox/flox}* mice exhibit a decrease in the power of prefrontal baseline high- γ (62–90 Hz) oscillations compared to their WT littermates.

(I) Novel object task. Just after the social interaction assay, the time each mouse spent with a novel object was measured ($n = 5$ mice per genotype, both groups). Data are presented as mean \pm SEM. * $p < 0.05$, ** $p < 0.01$.

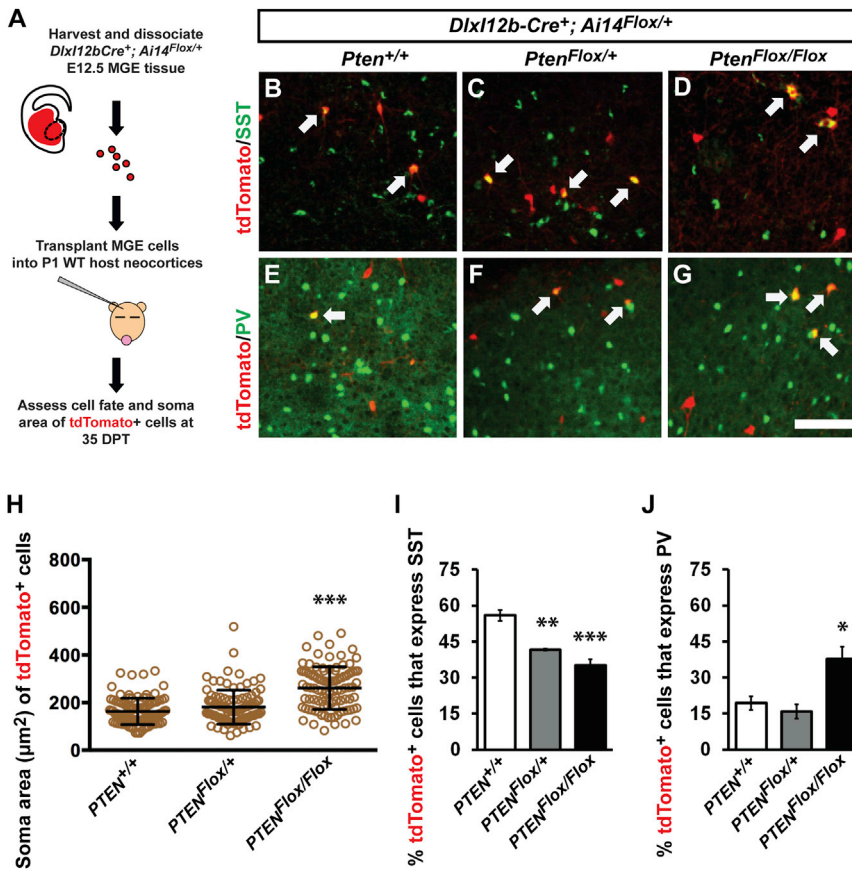


Figure 6. Cortical Interneurons Derived from Transplanted *Pten* cKO MGE Have Increased Soma Size and Increased PV⁺/SST⁺ Ratio

(A) Schema depicting the transplantation procedure. E12.5 *Dlx12b-Cre⁺; Ai14^{Flox/+}* MGE cells (tdTomato⁺) that were *Pten^{+/+}*, *Pten^{Flox/+}*, or *Pten^{Flox/Flox}* were transplanted into WT P1 neocortices and allowed to develop for 35 days posttransplant (DPT).

(B–G) Coronal immunofluorescent images of neocortices transplanted with *Pten^{+/+}*, *Pten^{Flox/+}*, or *Pten^{Flox/Flox}* MGE cells show coexpression of tdTomato and SST (B–D) or PV (E–G). Arrows point to coexpressing cells.

(H–J) Quantification of soma size of the tdTomato⁺ cells (H) and the proportion of tdTomato⁺ cells that express either SST (I) or PV (J).

Data are presented as mean ± SD (H) and ±SEM (I and J). **p* < 0.05, ***p* < 0.01, ****p* < 0.001. Scale bar in (G), 100 μm. See also Figure S4 and Table S3.

the phenotypes of the gene deletion. Moreover, by using the *Dlx12b* enhancer that drives expression in the majority of GABAergic cortical neurons (Potter et al., 2009), we could study the effects of alleles only in GABAergic lineages. To this end, we generated lentiviruses with the *Dlx12b* enhancer (Arguello et al., 2013; Vogt et al., 2014), followed by a β-globin minimal promoter driving *Cre* alone, with WT human *PTEN* or with *PTEN* ASD alleles (Figure S5A). To test the fidelity of this assay, five previously reported *PTEN* alleles, identified in patients with *PTEN*-related syndromes and diagnosed with ASD (Butler et al., 2005; Orrico et al., 2009), were chosen for comparison to WT *PTEN*. Each vector was expressed in HEK293T cells and assayed for Akt activity, via phosphorylation at Ser⁴⁷³ (Figure S5B). Expression of WT *PTEN* efficiently decreased the level of pAkt. However, none of the *PTEN* ASD mutants were able to efficiently inactivate Akt, suggesting that they are less functional than WT *PTEN*.

To assess the function of the *PTEN* ASD alleles in cortical interneuron development, we transduced MGE cells with the aforementioned viruses before transplantation (schema, Figure 7A). E12.5 MGE cells that were either *Ai14^{Flox/+}* (controls) or *Pten^{Flox/Flox}; Ai14^{Flox/+}* were transduced with *Dlx12b-Cre* lentiviruses (Figure S5A). These cells were then transplanted into P1 WT neocortices and developed in vivo until 35 DPT. *Cre* will result in the expression of tdTomato from the *Ai14* locus and will delete endogenous *Pten* from *Pten^{Flox/Flox}* MGE cells. Since

expression of WT *PTEN*, but not the *PTEN* ASD alleles, decreased the proportion of PV⁺ cells (Figures 7B–7I; *p* = 0.002), suggesting that *PTEN* dosage influences this phenotype. Next, we assessed if *PTEN* ASD alleles could complement the increased percentage of transplanted cells that are PV⁺ in *Pten* cKO MGE cells. Transduction of *Pten^{Flox/Flox}* MGE cells led to an increased % of PV⁺ cells compared to control cells with *Cre* only (Figures 7B, 7B', 7I, and 7J; Table S2), consistent with earlier data (Figures 1 and S2). Complementation with WT *PTEN* efficiently restored the percentage of PV⁺ cells to control levels (Figures 7C' and 7J; *p* = 0.0006). Notably, the *PTEN* ASD mutants were unable to complement the increased percentage of PV⁺ cells, and many were indistinguishable from *Cre* alone. Moreover, they differed from WT *PTEN* (Figures 7C'–7H' and 7J; *p* = 0.002 *Pten^{H118P}*, *p* = 0.003 *Pten^{Y176C}*, *p* = 0.0001 *Pten^{F241S}*, *p* = 0.005 *Pten^{D252G}*). While WT and *PTEN* ASD mutants showed clear distinctions, there was no evidence of a dominant-negative effect induced by *PTEN* ASD mutants when expressed in control MGE cells. These data showed a role for *PTEN* dosage in regulating PV⁺ interneuron ratios and demonstrated that *PTEN* ASD alleles are deficient in complementing this phenotype.

The percentage of transplanted cells that were SST⁺ was assessed in the same manner (Figures S6A–S6I). SST⁺ cells were reduced ~15% in *Pten^{Flox/Flox}* MGE cells compared to control cells transduced with *Cre* only (Figures S6H and S6I; Table S2), and the percentage of *Pten^{Flox/Flox}* cells that were SST⁺

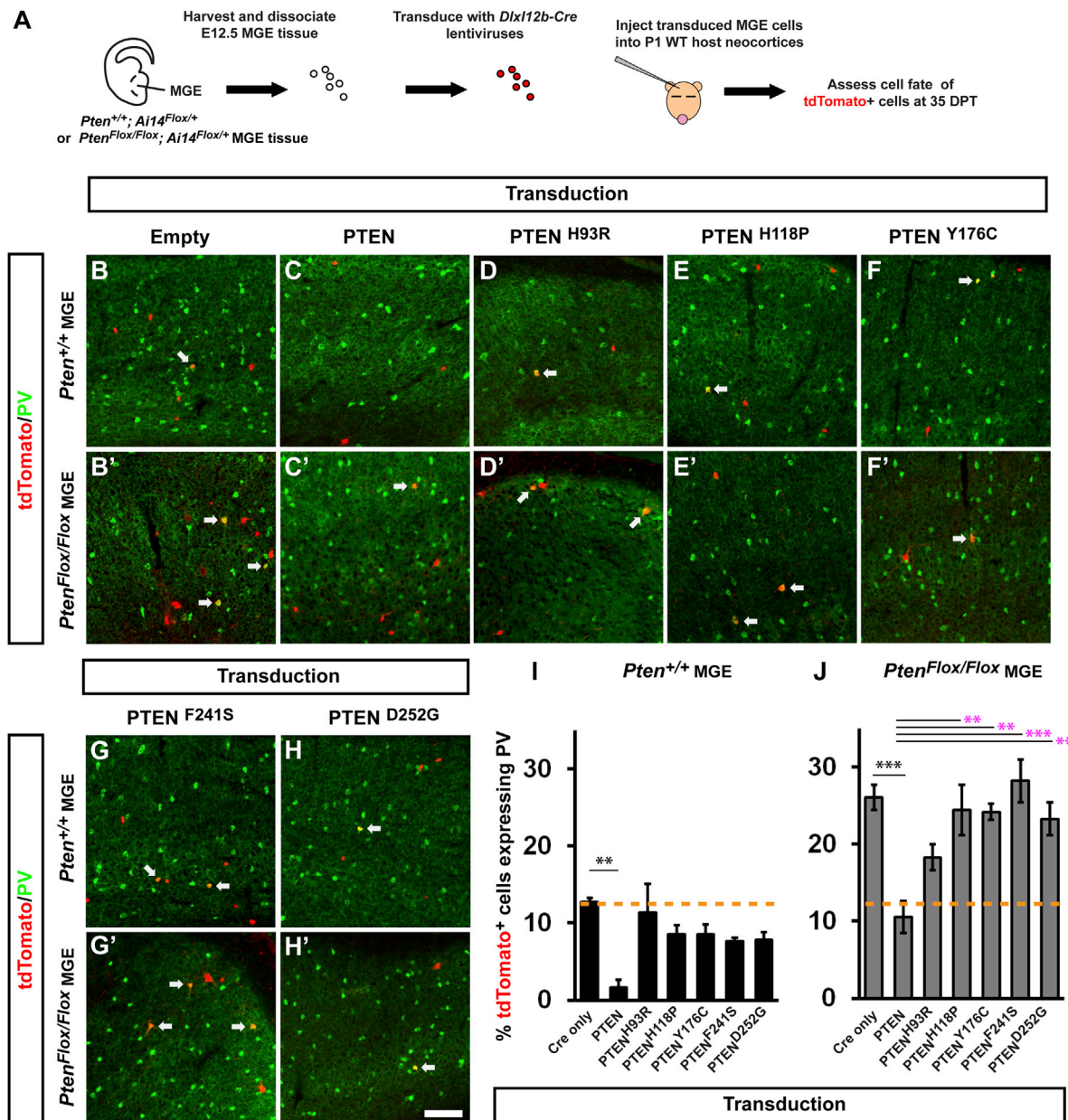


Figure 7. Complementation Assay Comparing WT and *PTEN* ASD Alleles Reveal Reduced Function of ASD Alleles in Regulating PV⁺ Interneuron Ratio

(A) Schema depicting the MGE transplantation and complementation assay. E12.5 control (*Pten*^{+/+}; *Ai14*^{Flox/+}) or (*Pten*^{Flox/Flox}; *Ai14*^{Flox/+}) MGE cells were transduced with a *Dlx12b-Cre-T2a-MCS* lentivirus that expresses either *Cre* only, or *Cre* with human WT *PTEN*, or a *PTEN* ASD allele, from the multiple cloning site (MCS). MGE cells were transplanted into a P1 wild-type (WT) neocortex and assessed at 35 DPT.

(B–H') Coronal immunofluorescent images of neocortices transplanted with transduced control (B–H) or *Pten*^{Flox/Flox} (B'–H') MGE cells show expression of tdTomato and PV at 35 DPT. Arrows point to coexpressing cells.

(I and J) Quantification of the % of tdTomato⁺ control (I) or *Pten*^{Flox/Flox} (J) transduced-MGE cells that coexpress PV.

Data are presented as mean ± SEM (n = 4, all groups). **p < 0.01, ***p < 0.001. Black asterisks, compared to *Cre*-only lentivirus; magenta asterisks, compared to WT *PTEN* lentivirus. Scale bar in (H'), 100 μm. See also Figures S5 and S6.

increased when complemented with WT *PTEN* (Figure S6I; p = 0.02). However, some of the *PTEN* ASD alleles did not complement the decreased percentage of SST⁺ cells (Figure S6I; p = 0.02 *PTEN*^{Y176C}, p = 0.009 *PTEN*^{D252G}).

Loss of *Pten* function increases cell size, including the cell bodies (somas) of neurons (Kwon et al., 2006; Figure 6H). Thus, we compared the function of WT and *PTEN* ASD alleles with regards to soma area. As expected, deletion of *Pten* by

transduction with *Cre* led to increased soma areas in *Pten*^{Flox/Flox} MGE cells (Figure S6K). Next, we quantified soma area after transduction with *PTEN* ASD alleles; each was less efficient than WT *PTEN* at preventing the increase in soma area of *Pten*^{Flox/Flox} MGE cells (Figure S6K; $p < 0.0001$ for WT *PTEN*, *PTEN*^{H118P} and *PTEN*^{Y176C}, $p = 0.04$ for *PTEN*^{F241S}, and $p = 0.0005$ for *PTEN*^{D252G}). Finally, we transduced *PTEN* or the ASD alleles into WT MGE cells and found no change in soma area with any allele (Figure S6J). Consistent with earlier data (Figure 7I and S6H), these results suggest that the *PTEN* ASD alleles do not act in a dominant fashion. Together, these data revealed a role for human *PTEN* ASD alleles in regulating cortical interneuron ratios and cell size and demonstrated a functional in vivo assay to test the impact each mutant imparts to development.

DISCUSSION

Pten is required to obtain normal numbers of SST⁺ and PV⁺ cortical interneurons, the two main subgroups of MGE-derived interneurons. Loss of *Pten* led to apoptosis that preferentially affected neonatal SST⁺ interneurons. This resulted in an increased PV⁺/SST⁺ ratio, as well as ectopic PV⁺ projections and a paucity of SST⁺ axons in cortical layer I. *Pten* mutants also had a decreased E/I ratio in neocortical layers II/III and reduced social behaviors. Finally, an MGE transplantation/complementation assay showed that *PTEN* ASD alleles were hypomorphic in vivo.

Pten Regulates the Number and Ratio of SST and PV Interneurons

Pten deletion in MGE progenitors of the VZ (via *Nkx2.1-Cre*) resulted in a greater reduction in SST⁺ compared to PV⁺ interneurons in the neocortex (Table S1). While this phenotype was also seen when *Pten* was deleted in the SVZ (via *Dlx12b-Cre*; Figure S2), no interneuron loss was observed using *SST-ires-Cre* (Figure 2), which begins to express as these cells become post-mitotic, suggesting that *Pten* regulation of interneuron numbers depends on its function in progenitors. The increased PV/SST ratio was also observed in MGE transplantation assays (Figures 6, 7, and S6), consistent with a cell-autonomous role for *Pten*.

The altered PV/SST ratio is likely due to preferential cell death of SST⁺ cells during late gestation and neonatal ages, rather than a change in cell fate or proliferation. In support of this, we did not observe changes in the proportion of SST⁺ MGE-derived cells at early embryonic ages (E12.5) or in proliferation (Figure S3). At E15.5, more SST⁺ interneurons occupied the lateral cortex and were depleted from the neocortex (Figure 3). By P0, there was elevated apoptosis that preferentially affected SST⁺ neurons in both the lateral and neocortex MZs, a time just before the major loss in interneurons was decreased in the neocortex (Figure 1H).

Alterations (increases and decreases) in cortical interneurons have been reported in ASD mouse mutants (Durand et al., 2012; Karayannis et al., 2014; Peñagarikano et al., 2011; Selby et al., 2007; Gogolla et al., 2014; Allegra et al., 2014). Thus, defects in interneuron numbers may be found in some forms of ASD, and the PV/SST ratio should be measured in ASD patients. Moreover, further work should be done in mice to elucidate the mechanisms that control the numbers of PV and SST interneurons.

Some insights have been garnered from the analysis of mouse transcription factor mutants that exhibit altered PV/SST ratios, including *Dlx1* (Cobos et al., 2005), *Lhx6* (Neves et al., 2013), *Npas1* and *Npas3* (Stanco et al., 2014), *Olig1* (Silbereis et al., 2014), and *Satb1* (Close et al., 2012; Denaxa et al., 2012). While the role of these transcription factors in neuropsychiatric disorders is obscure, alleles of some of these genes have been associated with disorders (Hamilton et al., 2005; Stanco et al., 2014).

Pten Regulates the Morphology and Connectivity of SST and PV Interneurons

Interestingly, PV⁺ processes ectopically grew into neocortical layer I, suggesting that *Pten* restrains the spatial distribution and perhaps connectivity of PV⁺ axons. Loss of *Pten* in excitatory neurons likewise results in overgrowth of their processes (Kwon et al., 2006). Given that layer I contains the apical dendrites of pyramidal neurons, the excessive PV⁺ processes could impact the nature and number of inhibitory inputs onto excitatory neurons. Indeed, loss of *Pten* in MGE-derived GABAergic cortical interneurons resulted in elevated spontaneous inhibitory tone on cortical layer II/III pyramidal neurons (Figure 4), despite the ~50% reduction in MGE-derived interneurons (Figure 1; Table S1). We hypothesize that the overgrowth of PV⁺ processes in layer I may underlie the increased inhibition. Interestingly, increased inhibitory tone has been observed in other mouse mutants of ASD genes that repress the PI3K/Akt/mTOR pathway, including *NF1* (Costa et al., 2002; Cui et al., 2008), suggesting that reducing the E/I ratio, through increased inhibition, may be an important mechanism underlying the effects of some ASD genes. Other ASD mouse models have increased E/I (Gogolla et al., 2014); thus, various mechanisms that disrupt E/I away from the optimal range, in either direction, may account for cortical dysfunction.

PV⁺ interneurons are necessary and sufficient for gamma oscillations (Cardin et al., 2009; Sohal et al., 2009), and various (depressed and elevated) alterations have been observed in individuals with ASD (Gandal et al., 2010; Orekhova et al., 2007; Wilson et al., 2007). In *Pten* cKO mice, we observed reduced gamma rhythms at rest and increased rhythms when performing a task (Figure 5). Finally, *Pten* mutants had deficits in social interaction (Figure 5), supporting the hypothesis that some behavioral and cognitive phenotypes may be caused by E/I imbalance (Rubenstein and Merzenich, 2003).

Loss of *Pten* in excitatory neurons led to phenotypes that were distinct from those observed from deletion in GABAergic cortical interneurons, including macrocephaly, increased excitation, and seizures (Kwon et al., 2006). Moreover, *Pten* deletion in either neuron type resulted in hyperactivated Akt and hypertrophy, suggesting that while different global phenotypes may be attributed to certain cell types, some cellular phenotypes were common between inhibitory and excitatory neurons (hyperactivated Akt and soma and neurite hypertrophy).

An In Vivo Complementation Assay to Screen Functional Changes in ASD Alleles

Due to the many risk alleles found in ASD (Murdoch and State, 2013; Tebbenkamp et al., 2014), we developed an efficient means to screen ASD alleles for functional deficits in vivo. This

was performed in cortical interneurons, a cell type implicated in ASD and other neuropsychiatric disorders. A standard way to study an ASD allele is to create a knockin mouse, which is a low-throughput process. Our complementation assay tests cell-autonomous effects of ASD alleles in ~2 months and can rapidly investigate molecular, developmental, morphological, and electrophysiological parameters *in vivo*. While this assay requires mouse null mutants, it is now relatively easy to obtain these animals. In addition, the modular design of the lentiviral vector (Figure S5) permits the use of any enhancer or promoter, which could facilitate assaying functions specific to cell type. Moreover, any gene can be inserted downstream of the *Cre* cassette. We suggest that this assay will be of great utility for *in vivo* functional characterization of any mutant allele.

Our assay showed that all five of the tested human *PTEN* ASD alleles were hypomorphic, based upon their reduced activity to rescue two phenotypes: increased soma area and PV/SST ratio (Figures 7 and S6). Consistent with our results, an assay of these alleles in yeast provided evidence that they had reduced phosphatase function, but not as low as *PTEN* alleles discovered in various cancers (Rodríguez-Escudero et al., 2011). Furthermore, these alleles did not have dominant functions when assayed in WT interneurons (Figures 7 and S6). In sum, our experiments delineate a major role for *PTEN* in the survival, connectivity, and PV/SST ratio of GABAergic cortical interneurons. These findings provide insights into how deficits in *PTEN* contribute to ASD and suggest that PI3K/Akt/mTor signaling differentially regulates PV and SST interneuron development.

EXPERIMENTAL PROCEDURES

Animals

All mice have been described previously: *Ai14* Cre-reporter (Madisen et al., 2010), *Nkx2.1-Cre* (Xu et al., 2008), *SST-IRES-Cre* (Taniguchi et al., 2011), *Dlx12b-Cre* (Potter et al., 2009), and *Pter^{fllox}* (Suzuki et al., 2001). Mice were initially on a mixed C57BL6/J, CD-1 background. All lines, except *SST-IRES-Cre*, were backcrossed to CD-1 for at least four generations before analysis. *SST-IRES-Cre* males were maintained on a C57Bl6/J background. For timed pregnancies, noon on the day of the vaginal plug was counted as E0.5. All animal care and procedures were performed according to the University of California at San Francisco Laboratory Animal Research Center guidelines.

Behavior

Open-Field Test

An individual mouse was placed near the wall-side of 50 × 50-cm open-field arena, and the movement of the mouse was recorded by a video camera for 10 min. The recorded video file was later analyzed with Any-Maze software (San Diego Instruments). Time in the center of the field (a 25 × 25-cm square), and distances traveled in the center and perimeter were measured. The open-field arena was cleaned with 70% ethanol and wiped with paper towels between each trial. Investigators were blind to genotype during scoring of videos.

Elevated Plus Maze Test

A mouse was placed at the junction of the open and closed arms, facing the arm opposite to the experimenter, of an apparatus with two open arms without walls (30 × 5 × 0.5 cm) across from each other and perpendicular to two closed arms with walls (30 × 5 × 15 cm) with a center platform (5 × 5 cm) and at a height of 40 cm above the floor. Mouse movement was recorded by video for 10 min and analyzed for the first 5 min. The video file was analyzed, and time and number of entries in the open arms of the apparatus were measured. The elevated plus maze apparatus arms were cleaned with 70% ethanol and wiped with paper towels between each trial. Investigators were blind to genotype during scoring of videos.

Social Interaction Task

Mice were connected to the EEG preamplifier and then habituated in their homecage for 15 min before beginning the task. After habituation, we recorded baseline EEG activity for 5 min. Then, we introduced an age-matched mouse (3–4 weeks old, same gender) into the homecage of the subject mouse and allowed the freely moving mice to interact for 5 min while continuing to record EEG activity. We recorded EEG using a time-locked video EEG monitoring system (Pinnacle Technology), enabling us to subsequently correlate periods of social interaction (defined as sniffing, close following, and allo-grooming) with specific time points in the EEG recording. Investigators were blind to genotype during scoring of videos.

Novel Object Task

Following the social interaction task, the subject mouse was presented with a novel object (50-ml Falcon tube cap) for 5 min, and the amount of time spent investigating the object was analyzed. Investigators were blind to genotype during scoring of videos.

Data analysis for EEGs was performed in Matlab (The MathWorks) using custom-written software. To analyze changes in power during the baseline period (which occurred just before the social interaction task), a two-way ANOVA was used and found to be significant for genotype if ($p < 0.001$), frequency if ($p < 0.001$), and genotype × frequency if ($p < 0.05$). The differences between genotypes for each frequency band was tested using Student's two-tailed, unpaired *t* tests. To analyze differences in social-interaction-evoked power, we used repeated-measures ANOVA with mouse, task condition (baseline versus social interaction), and genotype × condition (baseline versus social interaction) as factors.

Electrophysiology

Slice Preparation

Slice preparation and intracellular recordings were performed as previously described (Sohal and Huguenard, 2005). Detailed methods can be found in Supplemental Experimental Procedures.

Lentiviral production. Lentiviral production was performed as previously described (Vogt et al., 2014, 2015). Detailed methods can be found in Supplemental Experimental Procedures.

MGE transplantation. MGE transplantations were done as previously described (Vogt et al., 2014, 2015). A detailed description can be found in Supplemental Experimental Procedures.

SUPPLEMENTAL INFORMATION

Supplemental Information includes Supplemental Experimental Procedures, six figures, and three tables and can be found with this article online at <http://dx.doi.org/10.1016/j.celrep.2015.04.019>.

AUTHOR CONTRIBUTIONS

D.V., K.K.A.C., and A.T.L. performed experiments. All authors conceived experiments and wrote the manuscript.

ACKNOWLEDGMENTS

This work was supported by grants to J.L.R.R. from Autism Speaks, Nina Ireland, Weston Havens Foundation, NIMH R01 MH081880, and NIMH R37 MH049428. V.S.S. was supported by the Staglin Family and International Mental Health Research Organization, NIH DP2 MH100011, and NIMH R01 MH100292. K.K.A.C. was supported by a NARSAD Young Investigator Award from the Brain and Behavior Foundation. A.T.L. was supported by a Medical Scientist Training Program grant from NIGMS (GM07618). J.L.R.R. is a founding member and consultant for Neuron Therapeutics.

Received: October 15, 2014

Revised: February 22, 2015

Accepted: April 8, 2015

Published: April 30, 2015

REFERENCES

- Allegra, M., Genovesi, S., Maggia, M., Cenni, M.C., Zunino, G., Sgadò, P., Caleario, M., and Bozzi, Y. (2014). Altered GABAergic markers, increased binocularity and reduced plasticity in the visual cortex of Engrailed-2 knockout mice. *Front. Cell. Neurosci.* 8, 163.
- Alvarez-Dolado, M., Calcagnotto, M.E., Karkar, K.M., Southwell, D.G., Jones-Davis, D.M., Estrada, R.C., Rubenstein, J.L.R., Alvarez-Buylla, A., and Baraban, S.C. (2006). Cortical inhibition modified by embryonic neural precursors grafted into the postnatal brain. *J. Neurosci.* 26, 7380–7389.
- Anderson, S.A., Eisenstat, D.D., Shi, L., and Rubenstein, J.L. (1997). Interneuron migration from basal forebrain to neocortex: dependence on *Dlx* genes. *Science* 278, 474–476.
- Arguello, A., Yang, X., Vogt, D., Stanco, A., Rubenstein, J.L.R., and Cheyette, B.N.R. (2013). Dapper antagonist of catenin-1 cooperates with Dishevelled-1 during postsynaptic development in mouse forebrain GABAergic interneurons. *PLoS ONE* 8, e67679.
- Bourgeron, T. (2009). A synaptic trek to autism. *Curr. Opin. Neurobiol.* 19, 231–234.
- Butler, M.G., Dasouki, M.J., Zhou, X.-P., Talebizadeh, Z., Brown, M., Takahashi, T.N., Miles, J.H., Wang, C.H., Stratton, R., Pilarski, R., and Eng, C. (2005). Subset of individuals with autism spectrum disorders and extreme macrocephaly associated with germline PTEN tumour suppressor gene mutations. *J. Med. Genet.* 42, 318–321.
- Cardin, J.A., Carlén, M., Meletis, K., Knoblich, U., Zhang, F., Deisseroth, K., Tsai, L.-H., and Moore, C.I. (2009). Driving fast-spiking cells induces gamma rhythm and controls sensory responses. *Nature* 459, 663–667.
- Chao, H.-T., Chen, H., Samaco, R.C., Xue, M., Chahrour, M., Yoo, J., Neul, J.L., Gong, S., Lu, H.-C., Heintz, N., et al. (2010). Dysfunction in GABA signaling mediates autism-like stereotypies and Rett syndrome phenotypes. *Nature* 468, 263–269.
- Close, J., Xu, H., De Marco García, N., Batista-Brito, R., Rossignol, E., Rudy, B., and Fishell, G. (2012). *Satb1* is an activity-modulated transcription factor required for the terminal differentiation and connectivity of medial ganglionic eminence-derived cortical interneurons. *J. Neurosci.* 32, 17690–17705.
- Cobos, I., Calcagnotto, M.E., Vilaythong, A.J., Thwin, M.T., Noebels, J.L., Baraban, S.C., and Rubenstein, J.L. (2005). Mice lacking *Dlx1* show subtype-specific loss of interneurons, reduced inhibition and epilepsy. *Nat. Neurosci.* 8, 1059–1068.
- Costa, R.M., Federov, N.B., Kogan, J.H., Murphy, G.G., Stern, J., Ohno, M., Kucherlapati, R., Jacks, T., and Silva, A.J. (2002). Mechanism for the learning deficits in a mouse model of neurofibromatosis type 1. *Nature* 415, 526–530.
- Cui, Y., Costa, R.M., Murphy, G.G., Elgersma, Y., Zhu, Y., Gutmann, D.H., Parada, L.F., Mody, I., and Silva, A.J. (2008). Neurofibromin regulation of ERK signaling modulates GABA release and learning. *Cell* 135, 549–560.
- Denaxa, M., Kalaitzidou, M., Garefalaki, A., Achimastou, A., Lasrado, R., Maes, T., and Pachnis, V. (2012). Maturation-promoting activity of SATB1 in MGE-derived cortical interneurons. *Cell Rep.* 2, 1351–1362.
- Du, J., Zhang, L., Weiser, M., Rudy, B., and McBain, C.J. (1996). Developmental expression and functional characterization of the potassium-channel subunit Kv3.1b in parvalbumin-containing interneurons of the rat hippocampus. *J. Neurosci.* 16, 506–518.
- Durand, S., Patrizi, A., Quast, K.B., Hachigian, L., Pavlyuk, R., Saxena, A., Carninci, P., Hensch, T.K., and Fagiolini, M. (2012). NMDA receptor regulation prevents regression of visual cortical function in the absence of *Mecp2*. *Neuron* 76, 1078–1090.
- Fraser, M.M., Bayazitov, I.T., Zakharenko, S.S., and Baker, S.J. (2008). Phosphatase and tensin homolog, deleted on chromosome 10 deficiency in brain causes defects in synaptic structure, transmission and plasticity, and myelination abnormalities. *Neuroscience* 151, 476–488.
- Gandal, M.J., Edgar, J.C., Ehrlichman, R.S., Mehta, M., Roberts, T.P.L., and Siegel, S.J. (2010). Validating γ oscillations and delayed auditory responses as translational biomarkers of autism. *Biol. Psychiatry* 68, 1100–1106.
- Gogolla, N., Takesian, A.E., Feng, G., Fagiolini, M., and Hensch, T.K. (2014). Sensory integration in mouse insular cortex reflects GABA circuit maturation. *Neuron* 83, 894–905.
- Hamilton, S.P., Woo, J.M., Carlson, E.J., Ghanem, N., Ekker, M., and Rubenstein, J.L. (2005). Analysis of four *DLX* homeobox genes in autistic probands. *BMC Genet.* 6, 52.
- Han, S., Tai, C., Westenbroek, R.E., Yu, F.H., Cheah, C.S., Potter, G.B., Rubenstein, J.L., Scheuer, T., de la Iglesia, H.O., and Catterall, W.A. (2012). Autistic-like behaviour in *Scn1a*^{+/−} mice and rescue by enhanced GABA-mediated neurotransmission. *Nature* 489, 385–390.
- Huang, Z.J., Di Cristo, G., and Ango, F. (2007). Development of GABA innervation in the cerebral and cerebellar cortices. *Nat. Rev. Neurosci.* 8, 673–686.
- Karayannis, T., Au, E., Patel, J.C., Kruglikov, I., Markx, S., Delorme, R., Héron, D., Salomon, D., Glessner, J., Restituito, S., et al. (2014). *Cntnap4* differentially contributes to GABAergic and dopaminergic synaptic transmission. *Nature* 511, 236–240.
- Kölsch, V., Charest, P.G., and Firtel, R.A. (2008). The regulation of cell motility and chemotaxis by phospholipid signaling. *J. Cell Sci.* 121, 551–559.
- Kwon, C.H., Luikart, B.W., Powell, C.M., Zhou, J., Matheny, S.A., Zhang, W., Li, Y., Baker, S.J., and Parada, L.F. (2006). *Pten* regulates neuronal arborization and social interaction in mice. *Neuron* 50, 377–388.
- Ljungberg, M.C., Sunnen, C.N., Lugo, J.N., Anderson, A.E., and D'Arcangelo, G. (2009). Rapamycin suppresses seizures and neuronal hypertrophy in a mouse model of cortical dysplasia. *Dis. Model. Mech.* 2, 389–398.
- Luikart, B.W., Schnell, E., Washburn, E.K., Bensen, A.L., Tovar, K.R., and Westbrook, G.L. (2011). *Pten* knockdown in vivo increases excitatory drive onto dentate granule cells. *J. Neurosci.* 31, 4345–4354.
- Madisen, L., Zwingman, T.A., Sunkin, S.M., Oh, S.W., Zariwala, H.A., Gu, H., Ng, L.L., Palmiter, R.D., Hawrylycz, M.J., Jones, A.R., et al. (2010). A robust and high-throughput Cre reporting and characterization system for the whole mouse brain. *Nat. Neurosci.* 13, 133–140.
- Marui, T., Hashimoto, O., Nanba, E., Kato, C., Tochigi, M., Umekage, T., Ishijima, M., Kohda, K., Kato, N., and Sasaki, T. (2004). Association between the neurofibromatosis-1 (NF1) locus and autism in the Japanese population. *Am. J. Med. Genet. B. Neuropsychiatr. Genet.* 131B, 43–47.
- Mbarek, O., Marouillat, S., Martineau, J., Barthélémy, C., Müh, J.P., and Andres, C. (1999). Association study of the NF1 gene and autistic disorder. *Am. J. Med. Genet.* 88, 729–732.
- Miyoshi, G., Hjerling-Leffler, J., Karayannis, T., Sousa, V.H., Butt, S.J.B., Battiste, J., Johnson, J.E., Machold, R.P., and Fishell, G. (2010). Genetic fate mapping reveals that the caudal ganglionic eminence produces a large and diverse population of superficial cortical interneurons. *J. Neurosci.* 30, 1582–1594.
- Murdoch, J.D., and State, M.W. (2013). Recent developments in the genetics of autism spectrum disorders. *Curr. Opin. Genet. Dev.* 23, 310–315.
- Neves, G., Shah, M.M., Liodis, P., Achimastou, A., Denaxa, M., Roalfe, G., Sesay, A., Walker, M.C., and Pachnis, V. (2013). The LIM homeodomain protein *Lhx6* regulates maturation of interneurons and network excitability in the mammalian cortex. *Cereb. Cortex* 23, 1811–1823.
- O'Roak, B.J., Vives, L., Fu, W., Egertson, J.D., Stanaway, I.B., Phelps, I.G., Carvill, G., Kumar, A., Lee, C., Ankenman, K., et al. (2012). Multiplex targeted sequencing identifies recurrently mutated genes in autism spectrum disorders. *Science* 338, 1619–1622.
- Orekhova, E.V., Stroganova, T.A., Nygren, G., Tsetlin, M.M., Posikera, I.N., Gillberg, C., and Elam, M. (2007). Excess of high frequency electroencephalogram oscillations in boys with autism. *Biol. Psychiatry* 62, 1022–1029.
- Orrico, A., Galli, L., Buoni, S., Orsi, A., Vonella, G., and Sorrentino, V. (2009). Novel PTEN mutations in neurodevelopmental disorders and macrocephaly. *Clin. Genet.* 75, 195–198.
- Peñagarikano, O., Abrahams, B.S., Herman, E.I., Winden, K.D., Gdalyahu, A., Dong, H., Sonnenblick, L.I., Gruber, R., Almajano, J., Bragin, A., et al. (2011). Absence of CNTNAP2 leads to epilepsy, neuronal migration abnormalities, and core autism-related deficits. *Cell* 147, 235–246.

- Pesold, C., Liu, W.S., Guidotti, A., Costa, E., and Caruncho, H.J. (1999). Cortical bitufted, horizontal, and Martinotti cells preferentially express and secrete reelin into perineuronal nets, nonsynaptically modulating gene expression. *Proc. Natl. Acad. Sci. USA* *96*, 3217–3222.
- Potter, G.B., Petryniak, M.A., Shevchenko, E., McKinsey, G.L., Ekker, M., and Rubenstein, J.L.R. (2009). Generation of Cre-transgenic mice using Dlx1/Dlx2 enhancers and their characterization in GABAergic interneurons. *Mol. Cell. Neurosci.* *40*, 167–186.
- Rodríguez-Escudero, I., Oliver, M.D., Andrés-Pons, A., Molina, M., Cid, V.J., and Pulido, R. (2011). A comprehensive functional analysis of PTEN mutations: implications in tumor- and autism-related syndromes. *Hum. Mol. Genet.* *20*, 4132–4142.
- Rubenstein, J.L.R., and Merzenich, M.M. (2003). Model of autism: increased ratio of excitation/inhibition in key neural systems. *Genes Brain Behav.* *2*, 255–267.
- Selby, L., Zhang, C., and Sun, Q.Q. (2007). Major defects in neocortical GABAergic inhibitory circuits in mice lacking the fragile X mental retardation protein. *Neurosci. Lett.* *412*, 227–232.
- Silbereis, J.C., Nobuta, H., Tsai, H.H., Heine, V.M., McKinsey, G.L., Meijer, D.H., Howard, M.A., Petryniak, M.A., Potter, G.B., Alberta, J.A., et al. (2014). Olig1 function is required to repress *dlx1/2* and interneuron production in Mammalian brain. *Neuron* *81*, 574–587.
- Sohal, V.S., and Huguenard, J.R. (2005). Inhibitory coupling specifically generates emergent gamma oscillations in diverse cell types. *Proc. Natl. Acad. Sci. USA* *102*, 18638–18643.
- Sohal, V.S., Zhang, F., Yizhar, O., and Deisseroth, K. (2009). Parvalbumin neurons and gamma rhythms enhance cortical circuit performance. *Nature* *459*, 698–702.
- Stanco, A., Pla, R., Vogt, D., Chen, Y., Mandal, S., Walker, J., Hunt, R.F., Lindtner, S., Erdman, C.A., Pieper, A.A., et al. (2014). NPAS1 represses the generation of specific subtypes of cortical interneurons. *Neuron* *84*, 940–953.
- Stiles, B.L. (2009). Phosphatase and tensin homologue deleted on chromosome 10: extending its PTENacles. *Int. J. Biochem. Cell Biol.* *41*, 757–761.
- Suzuki, A., Yamaguchi, M.T., Ohteki, T., Sasaki, T., Kaisho, T., Kimura, Y., Yoshida, R., Wakeham, A., Higuchi, T., Fukumoto, M., et al. (2001). T cell-specific loss of Pten leads to defects in central and peripheral tolerance. *Immunity* *14*, 523–534.
- Taniguchi, H., He, M., Wu, P., Kim, S., Paik, R., Sugino, K., Kvitsiani, D., Fu, Y., Lu, J., Lin, Y., et al. (2011). A resource of Cre driver lines for genetic targeting of GABAergic neurons in cerebral cortex. *Neuron* *71*, 995–1013.
- Tebbenkamp, A.T.N., Willsey, A.J., State, M.W., and Sestan, N. (2014). The developmental transcriptome of the human brain: implications for neurodevelopmental disorders. *Curr. Opin. Neurol.* *27*, 149–156.
- Vogt, D., Hunt, R.F., Mandal, S., Sandberg, M., Silberberg, S.N., Nagasawa, T., Yang, Z., Baraban, S.C., and Rubenstein, J.L.R. (2014). Lhx6 directly regulates *Arx* and *CXCR7* to determine cortical interneuron fate and laminar position. *Neuron* *82*, 350–364.
- Vogt, D., Wu, P.-R., Sorrells, S.F., Arnold, C., Alvarez-Buylla, A., and Rubenstein, J.L.R. (2015). Viral-mediated labeling and transplantation of medial ganglionic eminence (MGE) cells for in vivo studies. *J. Vis. Exp.*, Published online April 23, 2015 <http://dx.doi.org/10.3791/52740>.
- Williams, M.R., DeSpensa, T., Jr., Li, M., Gullledge, A.T., and Luikart, B.W. (2015). Hyperactivity of newborn Pten knock-out neurons results from increased excitatory synaptic drive. *J. Neurosci.* *35*, 943–959.
- Wilson, T.W., Rojas, D.C., Reite, M.L., Teale, P.D., and Rogers, S.J. (2007). Children and adolescents with autism exhibit reduced MEG steady-state gamma responses. *Biol. Psychiatry* *62*, 192–197.
- Wiznitzer, M. (2004). Autism and tuberous sclerosis. *J. Child Neurol.* *19*, 675–679.
- Wonders, C.P., and Anderson, S.A. (2006). The origin and specification of cortical interneurons. *Nat. Rev. Neurosci.* *7*, 687–696.
- Xu, Q., Tam, M., and Anderson, S.A. (2008). Fate mapping Nkx2.1-lineage cells in the mouse telencephalon. *J. Comp. Neurol.* *506*, 16–29.
- Zhou, J., Blundell, J., Ogawa, S., Kwon, C.-H., Zhang, W., Sinton, C., Powell, C.M., and Parada, L.F. (2009). Pharmacological inhibition of mTORC1 suppresses anatomical, cellular, and behavioral abnormalities in neural-specific Pten knock-out mice. *J. Neurosci.* *29*, 1773–1783.